

Compact slit-based couplers for metal-dielectric-metal plasmonic waveguides

Yin Huang,^{1,2} Changjun Min,^{2,3} and Georgios Veronis^{1,2,*}

¹*Department of Electrical and Computer Engineering, Louisiana State University, Baton Rouge, Louisiana 70803, USA*

²*Center for Computation and Technology, Louisiana State University, Baton Rouge, Louisiana 70803, USA*

³*Current address: Institute of Modern Optics, Nankai University, Tianjin 300071, China*

*gveronis@lsu.edu

Abstract: We introduce compact wavelength-scale slit-based structures for coupling free space light into metal-dielectric-metal (MDM) subwavelength plasmonic waveguides. We first show that for a single slit structure the coupling efficiency is limited by a trade-off between the light power coupled into the slit, and the transmission of the slit-MDM waveguide junction. We next consider a two-section slit structure, and show that for such a structure the upper slit section enhances the coupling of the incident light into the lower slit section. The optimized two-section slit structure results in ~ 2.3 times enhancement of the coupling into the MDM plasmonic waveguide compared to the optimized single-slit structure. We finally consider a symmetric double-slit structure, and show that for such a structure the surface plasmons excited at the metal-air interfaces are partially coupled into the slits. Thus, the coupling of the incident light into the slits is greatly enhanced, and the optimized double-slit structure results in ~ 3.3 times coupling enhancement compared to the optimized single-slit structure. In all cases the coupler response is broadband.

© 2012 Optical Society of America

OCIS codes: (240.6680) Surface plasmons; (260.3910) Metal optics; (130.2790) Guided waves.

References and links

1. J. R. Krenn, B. Lamprecht, H. Ditlbacher, G. Schider, M. Salerno, A. Leitner, and F. R. Aussenegg, "Non-diffraction-limited light transport by gold nanowires," *Europhys. Lett.* **60**, 663–669 (2002).
2. S. A. Maier, P. G. Kik, H. A. Atwater, S. Meltzer, E. Harel, B. E. Koel, and A. A. G. Requicha, "Local detection of electromagnetic energy transport below the diffraction limit in metal nanoparticle plasmon waveguides," *Nat. Mater.* **2**, 229–232 (2003).
3. S. I. Bozhevolnyi, V. S. Volkov, E. Devaux, J. Y. Laluet, and T. W. Ebbesen, "Channel plasmon subwavelength waveguide components including interferometers and ring resonators," *Nature* **440**, 508–511 (2006).
4. R. Zia, M. D. Selker, P. B. Catrysse, and M. L. Brongersma, "Geometries and materials for subwavelength surface plasmon modes," *J. Opt. Soc. Am. A* **21**, 2442–2446 (2004).
5. G. Veronis and S. Fan, "Bends and splitters in subwavelength metal-dielectric-metal plasmonic waveguides," *Appl. Phys. Lett.* **87**, 131102 (2005).
6. A. Hosseini and Y. Massoud, "Nanoscale surface plasmon based resonator using rectangular geometry," *Appl. Phys. Lett.* **90**, 181102 (2007).
7. Y. Matsuzaki, T. Okamoto, M. Haraguchi, M. Fukui, and M. Nakagaki, "Characteristics of gap plasmon waveguide with stub structures," *Opt. Express* **16**, 16314–16325 (2008).

8. X. S. Lin and X. G. Huang, "Tooth-shaped plasmonic waveguide filters with nanometric sizes," *Opt. Lett.* **33**, 2874–2876 (2008).
9. D. M. Pozar, *Microwave Engineering* (Wiley, New York, 1998).
10. E. N. Economou, "Surface plasmons in thin films," *Phys. Rev.* **182**, 539–554 (1969).
11. G. Veronis and S. Fan, "Theoretical investigation of compact couplers between dielectric slab waveguides and two-dimensional metal-dielectric-metal plasmonic waveguides," *Opt. Express* **15**, 1211–1221 (2007).
12. E. Feigenbaum and M. Orenstein, "Modeling of complementary void plasmon waveguiding," *J. Lightwave Technol.* **25**, 2547–2562 (2007).
13. R. A. Wahsheh, Z. L. Lu, and M. A. G. Abushagur, "Nanoplasmonic couplers and splitters," *Opt. Express* **17**, 19033–19040 (2009).
14. R. X. Yang, R. A. Wahsheh, Z. L. Lu, and M. A. G. Abushagur, "Efficient light coupling between dielectric slot waveguide and plasmonic slot waveguide," *Opt. Lett.* **35**, 649–651 (2010).
15. J. Tian, S. Yu, W. Yan, and M. Qiu, "Broadband high-efficiency surface-plasmon-polariton coupler with silicon-metal interface," *Appl. Phys. Lett.* **95**, 013504 (2009).
16. C. Delacour, S. Blaize, P. Grosse, J. M. Fedeli, A. Bruyant, R. Salas-Montiel, G. Lerondel, and A. Chelnokov, "Efficient directional coupling between silicon and copper plasmonic nanoslot waveguides: toward metal-oxide-silicon nanophotonics," *Nano Lett.* **10**, 2922–2926 (2010).
17. M. J. Preiner, K. T. Shimizu, J. S. White, and N. A. Melosh, "Efficient optical coupling into metal-insulator-metal plasmon modes with subwavelength diffraction gratings," *Appl. Phys. Lett.* **92**, 113109 (2008).
18. J. A. Dionne, H. J. Lezec, and H. A. Atwater, "Highly confined photon transport in subwavelength metallic slot waveguides," *Nano Lett.* **6**, 1928–1932 (2006).
19. H. J. Lezec, J. A. Dionne, and H. A. Atwater, "Negative refraction at visible frequencies," *Science* **316**, 430–432 (2007).
20. S. I. Bozhevolnyi, *Plasmonic Nanoguides and Circuits* (World Scientific, 2009).
21. P. Neutens, P. V. Dorpe, I. D. Vlamincx, L. Lagae, and G. Borghs, "Electrical detection of confined gap plasmons in metal-insulator-metal waveguides," *Nature Photonics* **3**, 283–286 (2009).
22. K. Diest, J. A. Dionne, M. Spain, and H. A. Atwater, "Tunable color filters based on metal-insulator-metal resonators," *Nano Lett.* **9**, 2579–2583 (2009).
23. S. D. Wu and E. N. Glytsis, "Finite-number-of-periods holographic gratings with finite-width incident beams: analysis using the finite-difference frequency-domain method," *J. Opt. Soc. Am. A* **19**, 2018–2029 (2002).
24. G. Veronis, R. W. Dutton, and S. Fan, "Method for sensitivity analysis of photonic crystal devices," *Opt. Lett.* **29**, 2288–2290 (2004).
25. E. D. Palik, *Handbook of Optical Constants of Solids* (Academic, New York, 1985).
26. J. Jin, *The Finite Element Method in Electromagnetics* (Wiley, New York, 2002).
27. A. Taflov, *Computational Electrodynamics* (Artech House, Boston, 1995).
28. S. E. Kocabas, G. Veronis, D. A. B. Miller, and S. Fan, "Transmission line and equivalent circuit models for plasmonic waveguide components," *IEEE J. Sel. Topics Quantum Electron.* **14**, 1462–1472 (2008).
29. S. Ramo, J. R. Whinnery, and T. Van Duzer, *Fields and Waves in Communication Electronics* (Wiley, New York, 1994).
30. C. Min and G. Veronis, "Absorption switches in metal-dielectric-metal plasmonic waveguides," *Opt. Express* **17**, 10757–10766 (2009).
31. K. Krishnakumar, "Micro-genetic algorithms for stationary and non-stationary function optimization," *Proc. SPIE* **1196**, 289–296 (1989).
32. C. Min, L. Yang, and G. Veronis, "Microcavity enhanced optical absorption in subwavelength slits," *Opt. Express* **19**, 26850–26858 (2011).
33. L. Verslegers, Z. Yu, P. B. Catrysse, and S. Fan, "Temporal coupled-mode theory for resonant apertures," *J. Opt. Soc. Am. B* **27**, 1947–1956 (2010).
34. C. A. Balanis, *Antenna Theory: Analysis and Design*, 3rd ed. (Wiley, 2005).

1. Introduction

Plasmonic waveguides have shown the potential to guide subwavelength optical modes, the so-called surface plasmon polaritons, at metal-dielectric interfaces. Several different nanoscale plasmonic waveguiding structures have been proposed, such as metallic nanowires, metallic nanoparticle arrays, V-shaped grooves, and metal-dielectric-metal (MDM) waveguides [1–8]. Among these, MDM plasmonic waveguides, which are the optical analogue of microwave two-conductor transmission lines [9], are of particular interest because they support modes with deep subwavelength scale over a very wide range of frequencies extending from DC to visible [10]. Thus, MDM waveguides could provide an interface between conventional optics and

subwavelength electronic and optoelectronic devices.

For applications involving MDM plasmonic waveguides, it is essential to develop compact structures to couple light efficiently into such waveguides [11]. Several different couplers between MDM and dielectric waveguides have been investigated both theoretically and experimentally [11–16]. In addition, structures for coupling free space radiation into MDM waveguides have also been investigated. In particular, Preiner *et al.* [17] investigated subwavelength diffraction gratings as coupling structures into MDM waveguide modes. However, in diffraction grating structures several grating periods are required for efficient waveguide mode excitation, so that such structures need to be several microns long when designed to operate at frequencies around the optical communication wavelength ($\lambda_0 = 1.55 \mu\text{m}$). In addition, in several experimental investigations of MDM waveguides and devices, a single slit was used to couple light from free space into MDM plasmonic waveguides [18–22]. While single slit coupling structures are more compact, slit-based coupler designs have not been investigated in detail.

In this paper, we investigate compact wavelength-scale slit-based structures for coupling free space light into MDM plasmonic waveguides. We show that for a single slit structure the coupling efficiency is limited by a trade-off between the light power coupled into the slit, and the transmission of the slit-MDM waveguide junction. We next consider a two-section slit structure, and show that for such a structure the upper slit section enhances the coupling of the incident light into the lower slit section, by improving the impedance matching between the incident plane wave and the lower slit mode. The optimized two-section slit structure results in ~ 2.3 times enhancement of the coupling into the MDM plasmonic waveguide compared to the optimized single-slit structure. We then consider a symmetric double-slit structure. We show that for such a structure the surface plasmons excited at the metal-air interfaces are partially coupled into the slits, and thus the coupling of the incident light into the slits is greatly enhanced. The optimized double-slit structure results in ~ 3.3 times coupling enhancement compared to the optimized single-slit structure. Finally, we show that, while all incoupling structures are optimized at a single wavelength, the operation wavelength range for high coupling efficiency is broad.

The remainder of the paper is organized as follows. In Section 2, we first define the transmission cross section of the MDM plasmonic waveguide for a given coupling structure, and briefly describe the simulation method used for the analysis of the couplers. The results obtained for the single slit, two-section slit, and double slit coupling structures are presented in Subsections 2.1, 2.2, and 2.3, respectively. Finally, our conclusions are summarized in Section 3.

2. Results

We consider a silver-silica-silver MDM plasmonic waveguide in which the upper metal layer has a finite thickness (Fig. 1(a)). The minimum thickness of this metal layer is chosen to be 150 nm. For such a thickness, the field profile and wave vector of the fundamental TM mode supported by such a waveguide at optical frequencies are essentially identical to the ones of a MDM plasmonic waveguide with semi-infinite metal layers. We consider compact wavelength-scale structures for incoupling a normally incident plane wave from free space into the fundamental mode of the silver-silica-silver MDM plasmonic waveguide. In all cases, the total width of the incoupling structure is limited to less than $1.1 \mu\text{m}$, which approximately corresponds to one wavelength in silica ($\lambda_s = \lambda_0/n_s$, where $n_s = 1.44$), when operating at the optical communication wavelength ($\lambda_0 = 1.55 \mu\text{m}$).

Due to the symmetry of all coupling structures considered in this paper, the same amount of power couples into the left and right propagating silver-silica-silver MDM waveguide modes. In other words, half of the total incoupled power couples into each of the left and right propagating MDM waveguide modes. For comparison of different incoupling configurations, we define

the *transmission cross section* σ_T of the silver-silica-silver MDM waveguide as the total light power coupled into the right propagating fundamental TM mode of the waveguide, normalized by the incident plane wave power flux density [11]. In two dimensions, the transmission cross section is in the unit of length.

We use a two-dimensional finite-difference frequency-domain (FDFD) method [23, 24] to numerically calculate the transmission in the MDM plasmonic waveguide. This method allows us to directly use experimental data for the frequency-dependent dielectric constant of metals such as silver [25], including both the real and imaginary parts, with no approximation. Perfectly matched layer (PML) absorbing boundary conditions are used at all boundaries of the simulation domain [26]. We also use the total-field-scattered-field formulation to simulate the response of the structure to a normally incident plane wave input [27].

2.1. Single slit coupler

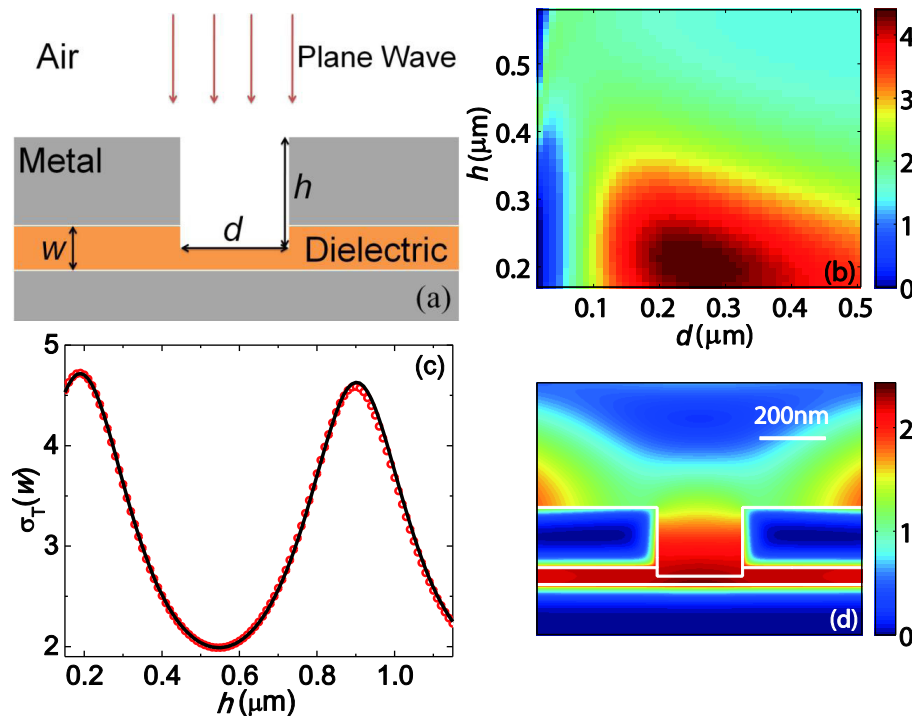


Fig. 1. (a) Schematic of a structure consisting of a single slit for incoupling a normally incident plane wave from free space into the fundamental mode of a MDM plasmonic waveguide. (b) Transmission cross section σ_T of the MDM plasmonic waveguide in units of w for the structure of Fig. 1(a) as a function of the slit width d and length h calculated using FDFD. Results are shown for a silver-silica-silver structure with $w = 50$ nm at $\lambda_0 = 1.55$ μm . (c) Transmission cross section σ_T for the structure of Fig. 1(a) as a function of the slit length h calculated using FDFD (red circles) and scattering matrix theory (black solid line). Results are shown for $d = 220$ nm. All other parameters are as in Fig. 1(b). (d) Profile of the magnetic field amplitude for the structure of Fig. 1(a) for $d = 250$ nm and $h = 205$ nm, normalized with respect to the field amplitude of the incident plane wave. All other parameters are as in Fig. 1(b).

We first consider a structure consisting of a single slit for incoupling a normally incident

plane wave from free space into the fundamental mode of the silver-silica-silver MDM plasmonic waveguide with dielectric core thickness w . The slit extends half way into the dielectric core of the MDM waveguide (Fig. 1(a)). In Fig. 1(b), we show the transmission cross section σ_T of the silver-silica-silver MDM waveguide in units of w for the single slit structure of Fig. 1(a) as a function of the width d and length h of the slit. For the range of parameters shown, we observe one transmission peak. The maximum cross section of $\sigma_T \sim 4.67w$ is obtained for such an incoupling structure at $d = 250$ nm and $h = 205$ nm (Fig. 1(b)).

Both the silver-silica-silver MDM waveguide and the silver-air-silver slit have subwavelength widths, so that only the fundamental TM mode is propagating in them. Thus, we can use single-mode scattering matrix theory to account for the behavior of the system [28]. We use FDFD to numerically extract the transmission cross section σ_{T_1} of a silver-air-silver MDM waveguide with air core thickness d (Fig. 2(a)). We also use FDFD to extract the complex magnetic field reflection coefficient r_1 and transmission coefficient t_1 of the fundamental mode of a silver-air-silver MDM waveguide at the T-shaped junction with a silver-silica-silver MDM waveguide (Fig. 2(b)), as well as the reflection coefficient r_2 at the interface between the silver-air-silver MDM waveguide and air (Fig. 2(c)).

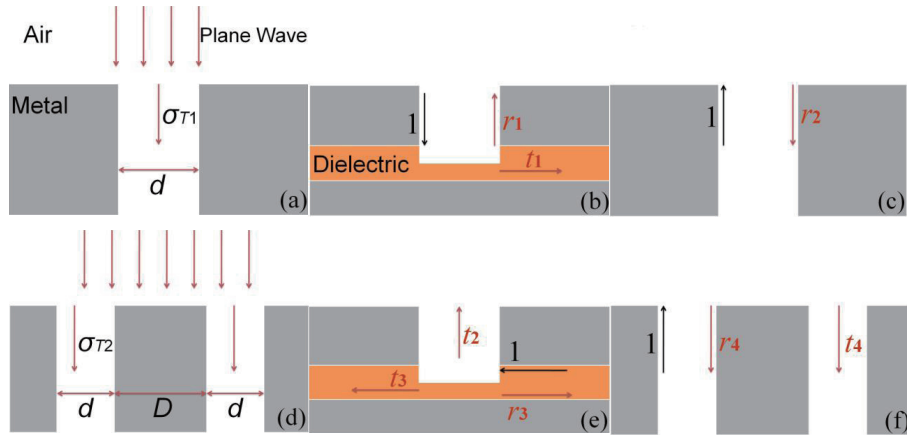


Fig. 2. (a) Schematic defining the transmission cross section σ_{T_1} of a semi-infinite MDM waveguide when a plane wave is normally incident on it. (b) Schematic defining the reflection coefficient r_1 , and transmission coefficient t_1 when the fundamental TM mode of a metal-air-metal waveguide is incident at the junction with a metal-dielectric-metal waveguide. (c) Schematic defining the reflection coefficient r_2 of the fundamental TM mode of a MDM waveguide at the waveguide/air interface. (d) Schematic defining the transmission cross section σ_{T_2} of two semi-infinite MDM waveguides when a plane wave is normally incident on them. (e) Schematic defining the reflection coefficient r_3 , and transmission coefficients t_2 , t_3 when the fundamental TM mode of a metal-dielectric-metal waveguide is incident at the junction with a metal-air-metal waveguide. (f) Schematic of a structure consisting of two semi-infinite MDM waveguides defining the reflection coefficient r_4 of the fundamental TM mode of one of the MDM waveguides at the waveguide/air interface, and the transmission coefficient t_4 into the other MDM waveguide.

The transmission cross section σ_T of the silver-silica-silver MDM waveguide for the single slit structure of Fig. 1(a) can then be calculated using scattering matrix theory as [28]:

$$\sigma_T = \sigma_{T_1} \eta_{\text{res}_1} T_{\text{splitter}}, \quad (1)$$

where $T_{\text{splitter}} = |t_1|^2$ is the power transmission coefficient of the T-shaped junction of Fig. 2(b),

$\eta_{\text{res}_1} = \left| \frac{\exp(-\gamma_1 h)}{1 - r_1 r_2 \exp(-2\gamma_1 h)} \right|^2$ is the resonance enhancement factor associated with the silver-air-silver slit resonance, and $\gamma_1 = \alpha_1 + i\beta_1$ is the complex wave vector of the fundamental propagating TM mode in a silver-air-silver MDM waveguide with air core thickness d . We note that η_{res_1} is a function of the reflection coefficients r_1 and r_2 at both sides of the silver-air-silver slit. We also observe that the resonance enhancement factor η_{res_1} exhibits a maximum when the slit Fabry-Pérot resonance condition $\arg(r_1) + \arg(r_2) - 2\beta_1 h = -2m\pi$ is satisfied, where m is an integer. Thus, for a given silver-air-silver slit width d , the transmission cross section σ_T of the silver-silica-silver MDM waveguide is maximized for slit lengths h which satisfy the above Fabry-Pérot resonance condition.

In Fig. 1(c), we show the transmission cross section σ_T of the silver-silica-silver MDM waveguide for the single slit structure of Fig. 1(a) as a function of the slit length h calculated using FDFD. We observe that, as the slit length h increases, the transmission cross section σ_T exhibits peaks, corresponding to the Fabry-Pérot resonances in the slit. The maximum transmission cross section σ_T is obtained at the first peak associated with the first Fabry-Pérot resonance in the slit. In Fig. 1(c), we also show σ_T calculated using scattering matrix theory (Eq. (1)). We observe that there is excellent agreement between the scattering matrix theory results and the exact results obtained using FDFD.

For the optimized single slit structure ($d = 250$ nm, $h = 205$ nm), the transmission cross section σ_{T_1} of the corresponding silver-air-silver MDM waveguide with air core thickness $d = 250$ nm (Fig. 2(a)) is $\sim 7.71w = 385.5$ nm (Table 1). In other words, the silver-air-silver subwavelength MDM waveguide collects light from an area significantly larger than its geometric cross-sectional area [11]. In addition, for the optimized single slit structure the power transmission coefficient of the T -shaped junction is $T_{\text{splitter}} \sim 0.37$, and the resonance enhancement factor is $\eta_{\text{res}_1} \sim 1.64$ (Table 1). Thus, $\sim 2 \times 37 = 74\%$ of the incident power at the junction is transmitted to the left and right propagating modes of the silver-silica-silver MDM waveguide.

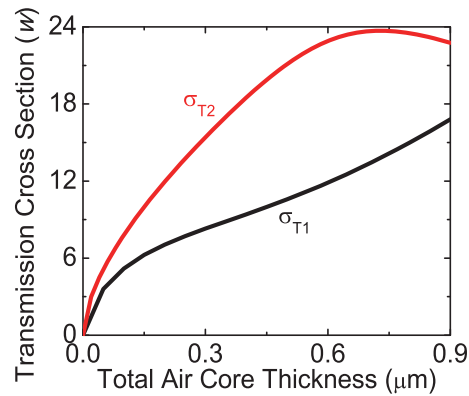


Fig. 3. Transmission cross sections (in units of $w = 50$ nm) of a single silver-air-silver MDM waveguide σ_{T_1} (Fig. 2(a)), and of a double silver-air-silver MDM waveguide σ_{T_2} (Fig. 2(d)), as a function of their total air core thickness (d for the single and $2d$ for the double waveguide). The total width of the double waveguide is $2d + D = 1.1 \mu\text{m}$.

In Fig. 3, we show the transmission cross section σ_{T_1} of a silver-air-silver MDM waveguide (Fig. 2(a)) as a function of the waveguide air core thickness d . We observe that, as expected, σ_{T_1} increases monotonically as the thickness d increases. In other words, the light power collected by the waveguide increases as the air core thickness of the waveguide increases. On the other hand, the properties of the T -shaped junction (Fig. 2(b)) can be described using the concept of characteristic impedance and transmission line theory [5, 9, 29]. Based on transmission line

Table 1. Transmission cross sections $\sigma_{T_{1/2}}$ and σ_T in units of w , power transmission coefficient of the T -shaped junction T_{splitter} , and resonance enhancement factors $\eta_{\text{res}_{1/2}}$ calculated using scattering matrix theory. Results are shown for the optimized single slit, two-section slit, and double-slit structures of Figs. 1(a), 4(a), and 5(a), respectively.

	Single slit	Two-section slit	Double-slit
$\sigma_{T_{1/2}}(w)$	7.71	12.33	18.49
T_{splitter}	0.37	0.28	0.41
$\eta_{\text{res}_{1/2}}$	1.64	3.11	2.02
$\sigma_T(w)$	4.67	10.75	15.29

theory, the structure is equivalent to the junction of three transmission lines. The load connected to the input transmission line at the junction consists of the series combination of the two output transmission lines. The characteristic impedances of the input and output transmission lines are $Z_1 = \frac{\gamma_1}{j\omega\epsilon_0}d$ and $Z_2 = \frac{\gamma_2}{j\omega\epsilon}w$, respectively, where $\gamma_2 = \alpha_2 + i\beta_2$ is the complex wave vector of the fundamental propagating TM mode in a silver-silica-silver MDM waveguide with dielectric core thickness w , and ϵ is the dielectric permittivity of silica [5, 30]. Thus, the equivalent load impedance is $Z_L = 2Z_2$, and the maximum transmission coefficient T_{splitter} is obtained when the impedance matching condition $Z_1 = Z_L = 2Z_2$ is satisfied. The transmission coefficient T_{splitter} of the T -shaped junction (Fig. 2(b)) therefore does not increase monotonically with d . As a result, the coupling efficiency of the single slit structure is limited by a trade-off between the power incident at the slit-MDM waveguide junction, and the transmission coefficient T_{splitter} of the T -shaped junction. More specifically, the width of the optimized single slit is $d = 250$ nm, as mentioned above. If the slit width d decreased, the impedance matching between the silver-air-silver MDM input waveguide and the two silver-silica-silver MDM output waveguides would improve, and T_{splitter} therefore would increase. However, if d decreased, the transmission cross section σ_{T_1} of the silver-air-silver MDM waveguide would decrease (Fig. 3). In addition, the reflectivity $|r_1|^2$ at the bottom side of the slit, and therefore the resonance enhancement factor η_{res_1} would also decrease. Thus, the power incident at the junction between the slit and the silver-silica-silver MDM waveguide would decrease.

In Fig. 1(d), we show the magnetic field profile for the structure of Fig. 1(a) when the slit dimensions are optimized for maximum transmission cross section σ_T . We observe that, since the transmission cross section of the silver-silica-silver MDM waveguide $\sigma_T \sim 4.67w$ is larger than its geometrical cross-section w , the field in the MDM waveguide is enhanced with respect to the incident plane wave field. We find that the maximum magnetic field amplitude enhancement in the silver-silica-silver waveguide with respect to the incident plane wave is ~ 2.4 (Fig. 1(d)).

2.2. Two-section slit coupler

To enhance the transmission cross section σ_T of the silver-silica-silver MDM plasmonic waveguide, we next consider a structure consisting of a two-section slit for incoupling light into the waveguide (Fig. 4(a)). The lengths h_1 , h_2 and widths d_1 , d_2 of these slit sections are optimized using a genetic global optimization algorithm in combination with FDFD [11, 31] to maximize the transmission cross section σ_T of the silver-silica-silver MDM waveguide. As before, the width of the incoupling structure is limited to less than $1.1\mu\text{m}$. Using this approach, the maximum transmission cross section of the silver-silica-silver MDM waveguide for such a two-section slit structure is found to be $\sigma_T \sim 10.75w$ (Table 1) for $d_1 = 410$ nm, $d_2 = 1100$ nm, $h_1 = 230$ nm, and $h_2 = 540$ nm.

We observe that for such a structure the transmission cross section of the corresponding

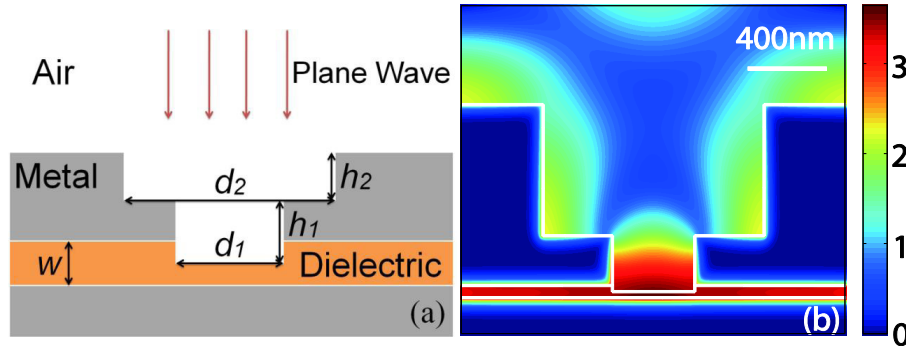


Fig. 4. (a) Schematic of a structure consisting of a two-section slit for incoupling a normally incident plane wave from free space into the fundamental mode of a MDM plasmonic waveguide. (b) Profile of the magnetic field amplitude for the optimized structure of Fig. 4(a) with $d_1 = 410$ nm, $d_2 = 1100$ nm, $h_1 = 230$ nm, and $h_2 = 540$ nm, normalized with respect to the field amplitude of the incident plane wave. All other parameters are as in Fig. 1(b).

silver-air-silver MDM waveguide (with air core thickness d_1) is $\sigma_{T_1} \sim 12.33w$ (Table 1), which is ~ 1.6 times larger compared to the optimized single slit coupler. In other words, the upper slit section can enhance the coupling of the incident light into the lower slit section, by improving the impedance matching between the incident plane wave and the lower slit mode [32]. In addition, the resonance enhancement factor of the optimized two-section slit structure is $\eta_{\text{res}_1} \sim 3.11$ (Table 1), which is ~ 1.9 times larger compared to the optimized single slit coupler. We found that the increase in the resonance enhancement factor η_{res_1} of this two-section slit structure is due to larger reflectivities $|r_1|^2$ and $|r_2|^2$ at both sides of the lower slit section compared to the optimized single slit coupler. On the other hand, the transmission coefficient of the T -shaped junction for the optimized two-section slit structure of Fig. 4(a) is $T_{\text{splitter}} \sim 0.28$ (Table 1), which is ~ 1.3 times smaller than the one of the optimized single slit structure. This is due to larger mismatch between the characteristic impedance of the input waveguide Z_1 and the load impedance $Z_L = 2Z_2$ at the T -shaped junction. Thus, overall the use of an optimized two-section slit coupler (Fig. 4(a)) results in $1.6 \times 1.9 / 1.3 \simeq 2.3$ times larger transmission cross section σ_T of the silver-silica-silver MDM waveguide compared to the single-slit coupler case (Fig. 1(a)). In Fig. 4(b), we show the magnetic field profile for the structure of Fig. 4(a) with dimensions optimized for maximum transmission cross section σ_T of the silver-silica-silver MDM waveguide. The field in the narrower lower slit section is stronger than the field in the upper slit section. The maximum magnetic field amplitude enhancement in the silver-silica-silver MDM waveguide with respect to the incident plane wave is ~ 3.6 (Fig. 4(b)).

2.3. Double-slit coupler

To further enhance the transmission cross section σ_T of the silver-silica-silver MDM plasmonic waveguide, we consider a symmetric double-slit structure for incoupling light into the waveguide (Fig. 5(a)). As before, the total width $2d + D$ of the incoupling structure is limited to less than $1.1 \mu\text{m}$. For such a double-slit coupling structure we found that, if $2d + D \leq 1.1 \mu\text{m}$, the maximum transmission cross section σ_T is obtained when $2d + D = 1.1 \mu\text{m}$. In the following we therefore set $2d + D = 1.1 \mu\text{m}$. In Fig. 5(b), we show the transmission cross section σ_T of the silver-silica-silver MDM waveguide in units of w for the structure of Fig. 5(a) as a function of the width d and length h of the slits. For the range of parameters shown, we observe one transmission peak in the silver-silica-silver MDM waveguide. The maximum transmission cross

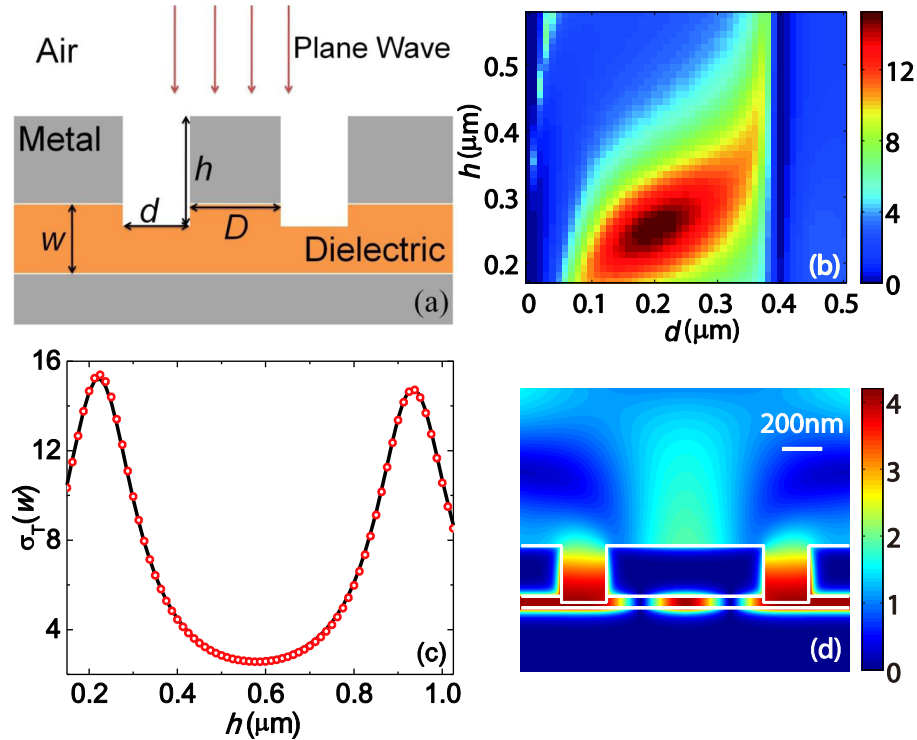


Fig. 5. (a) Schematic of a double-slit structure for incoupling a normally incident plane wave from free space into the fundamental mode of a MDM plasmonic waveguide. (b) Transmission cross section σ_T of the MDM plasmonic waveguide in units of w for the structure of Fig. 5(a) as a function of the slit width d and length h calculated using FDFD. The total width of the incoupling structure is $2d + D = 1.1\mu\text{m}$. All other parameters are as in Fig. 1(b). (c) Transmission cross section σ_T for the structure of Fig. 5(a) as a function of the slit length h calculated using FDFD (red circles) and scattering matrix theory (black solid line). Results are shown for $d = 220\text{ nm}$. All other parameters are as in Fig. 5(b). (d) Profile of the magnetic field amplitude for the structure of Fig. 5(a) for $d = 200\text{ nm}$ and $h = 250\text{ nm}$, normalized with respect to the field amplitude of the incident plane wave. All other parameters are as in Fig. 5(b).

section of $\sigma_T \sim 15.29w$ is obtained for such an incoupling structure at $d = 200\text{ nm}$ ($D = 700\text{ nm}$) and $h = 250\text{ nm}$. We also note that for $d \sim 400\text{ nm}$ ($D \sim 300\text{ nm}$) the transmission into the silver-silica-silver MDM waveguide is almost zero (Fig. 5(b)). We found that this is due to the fact that for a slit distance of $D \sim 300\text{ nm}$ the incident light strongly couples into the silver-silica-silver waveguide resonator between the slits. In addition, there is almost no light coupled into the left and right propagating modes of the silver-silica-silver MDM waveguide, due to destructive interference between the wave directly coupled through the slit, and the wave coupled through the silver-silica-silver waveguide resonator.

We use again single-mode scattering matrix theory to account for the behavior of the system. We use FDFD to numerically extract the transmission cross section σ_{T_2} of a double silver-air-silver MDM waveguide as in Fig. 2(d). We also use FDFD to extract the complex magnetic field reflection coefficient r_3 and transmission coefficients t_2, t_3 of the fundamental mode of a silver-silica-silver MDM waveguide at the T-shaped junction with a silver-air-silver MDM waveguide (Fig. 2(e)). Note that $t_1 = t_2$ due to reciprocity [9]. Finally, we also extract the re-

flection coefficient r_4 at the interface between the silver-air-silver MDM waveguide and air, and the transmission coefficient t_4 into the other MDM waveguide, for the double MDM waveguide structure (Fig. 2(f)). The transmission cross section σ_T of the silver-silica-silver MDM plasmonic waveguide for the double-slit coupling structure of Fig. 5(a) is then calculated using scattering matrix theory as:

$$\sigma_T = \sigma_{T_2} \eta_{\text{res}_2} T_{\text{splitter}}, \quad (2)$$

where, as before, $T_{\text{splitter}} = |t_1|^2 = |t_2|^2$ is the power transmission coefficient of the T -shaped junction, $\eta_{\text{res}_2} = \left| \frac{\exp(-\gamma_1 h)(1+t_3 A)}{1-(r_1+t_1 t_2 A)(r_4+t_4) \exp(-2\gamma_1 h)} \right|^2$ is the resonance enhancement factor associated with the complex resonator formed by the two silver-air-silver slits and the silver-silica-silver MDM waveguide resonator of length D between them, and $A = \frac{\exp(-\gamma_2 D)+r_3 \exp(-2\gamma_2 D)}{1-r_3^2 \exp(-2\gamma_2 D)}$. Thus, we observe that the resonant enhancement factor η_{res_2} for such a complex resonator is similar to that of a Fabry-Pérot resonator with effective reflectivities $r_{\text{eff}_1} = r_1 + t_1 t_2 A$ and $r_{\text{eff}_2} = r_4 + t_4$.

In Fig. 5(c), we show the transmission cross section σ_T for the structure of Fig. 5(a) as a function of the slit length h calculated using FDFD. We observe that, as the slit length h increases, the transmission cross section σ_T exhibits peaks, associated with the resonances of the double-slit structure. The maximum transmission cross section σ_T is obtained at the first peak associated with the first resonant length of the slits. In Fig. 5(c), we also show σ_T calculated using scattering matrix theory (Eq. (2)). We observe that there is excellent agreement between the scattering matrix theory results and the exact results obtained using FDFD.

We found that for the optimized double-slit structure the transmission cross section of the corresponding double silver-air-silver MDM waveguide (Fig. 2(d)) is $\sigma_{T_2} \sim 18.49w$ (Table 1), which is ~ 2.4 times larger compared to the transmission cross section $\sigma_{T_1} \sim 7.71w$ of the single silver-air-silver MDM waveguide corresponding to the optimized single slit coupler (Fig. 2(a)). In Fig. 3 we show the transmission cross sections of a single silver-air-silver MDM waveguide σ_{T_1} (Fig. 2(a)), and of a double silver-air-silver MDM waveguide σ_{T_2} (Fig. 2(d)) as a function of their total air core thickness (d for the single and $2d$ for the double waveguide). We observe that a double silver-air-silver MDM waveguide collects more light than a single silver-air-silver MDM waveguide with the same total air core thickness. This is due to the fact that, when a plane wave is incident on a semi-infinite MDM waveguide, surface plasmon waves are excited at the air-metal interfaces. In the double MDM waveguide structure (Fig. 2(d)), the power of these surface plasmon waves is partially coupled into the MDM waveguides, thus increasing the total light power collected by the structure. In addition, the resonance enhancement factor of the optimized double-slit structure $\eta_{\text{res}_2} \sim 2.02$ (Table 1) is slightly larger than the resonance enhancement factor of the optimized single slit coupler ($\eta_{\text{res}_1} \sim 1.64$). Overall, the use of an optimized double-slit coupler (Fig. 5(a)) results in ~ 3.3 times larger transmission cross section σ_T of the silver-silica-silver MDM waveguide compared to the optimized single-slit coupler case (Fig. 1(a)). In Fig. 5(d), we show the magnetic field profile for the structure of Fig. 5(a) with dimensions optimized for maximum transmission cross section. The maximum magnetic field amplitude enhancement in the silver-silica-silver waveguide with respect to the incident plane wave is ~ 4.2 .

The incoupling structures were all optimized at a single wavelength of $\lambda_0 = 1.55 \mu\text{m}$. In Fig. 6, we show the transmission cross section σ_T of the silver-silica-silver MDM plasmonic waveguide as a function of frequency for the optimized structures of Fig. 1(d) (single slit), Fig. 4(b) (two-section slit), and Fig. 5(d) (double slit). We observe that the operation frequency range for high transmission is broad. This is due to the fact that in all cases the enhanced transmission is not associated with any strong resonances. In other words, the quality factors Q of the slit coupling structures are low. In Fig. 6 we also show the transmission cross section σ_T for the double-slit structure, if the metal in the MDM waveguide is lossless ($\epsilon_{\text{metal}} = \text{Re}(\epsilon_{\text{metal}})$),

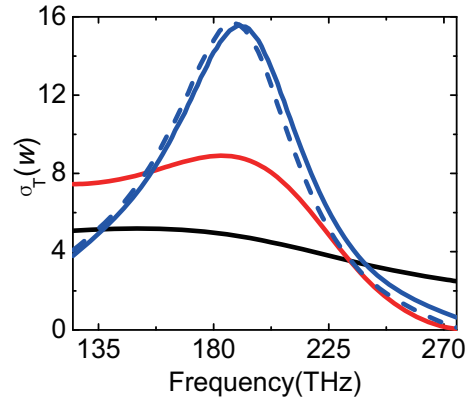


Fig. 6. Transmission cross section σ_T spectra in units of w for the three optimized incoupling structures in Figs. 1(a) (single slit), 4(a) (two-section slit), and 5(a) (double slit). Results are shown for the structure of Fig. 1(a) with $d = 250$ nm, $h = 205$ nm (black line), for the structure of Fig. 4(a) with $d_1 = 410$ nm, $d_2 = 1100$ nm, $h_1 = 230$ nm, and $h_2 = 540$ nm (red line), and for the structure of Fig. 5(a) with $d = 200$ nm, $h = 250$ nm (blue line). Also shown are the transmission cross section σ_T spectra for the double-slit structure (Fig. 5(a)), if the metal in the MDM waveguide is lossless (blue dashed line). All other parameters are as in Fig. 1(b).

neglecting the imaginary part of the dielectric permittivity $\text{Im}(\epsilon_{\text{metal}})$). We observe that material losses in the metal do not significantly affect the transmission efficiency of the incoupling structures. This is due to the fact that the dimensions of the incoupling structures are much smaller than the propagation lengths of the fundamental TM modes in the silver-silica-silver and the silver-air-silver waveguides. We found that neither the coupling of the incident light into the silver-air-silver slits nor the coupling between the slits and the silver-silica-silver MDM plasmonic waveguide are significantly affected by material losses in the metal.

3. Conclusions

In this paper, we investigated compact slit-based structures for coupling free space light into silver-silica-silver MDM plasmonic waveguides. In all cases, the total width of the incoupling structure was limited to less than $1.1 \mu\text{m}$, which approximately corresponds to one wavelength in silica $\lambda_s = \lambda_0/n_s$, when operating at $\lambda_0 = 1.55 \mu\text{m}$. We first considered a coupling structure consisting of a single slit extending half way into the dielectric core of the MDM waveguide. We found that the coupling efficiency of such a single slit structure is limited by a trade-off between the light power coupled into the slit, and the transmission of the slit-MDM waveguide T -shaped junction.

To enhance the coupling into the silver-silica-silver MDM plasmonic waveguide, we next considered a two-section slit structure. We found that for such a structure the upper slit section enhances the coupling of the incident light into the lower slit section, by improving the impedance matching between the incident plane wave and the lower slit mode. In addition, the use of the optimized two-section slit structure increases the reflectivities at both sides of the lower slit section, and therefore the resonance enhancement factor. On the other hand, the transmission of the T -shaped junction for the optimized two-section slit structure is smaller than the one of the optimized single slit structure. Overall, the use of an optimized two-section slit coupler resulted in ~ 2.3 times enhancement of the coupling into the MDM plasmonic waveguide compared to the optimized single-slit coupler.

To further enhance the coupling into the silver-silica-silver MDM plasmonic waveguide, we considered a symmetric double-slit structure. We found that such a structure greatly enhances the coupling of the incident light into the slits. This is due to the fact that the incident light excites surface plasmons at the air-metal interfaces. In the case of a double-slit structure these plasmons are partially coupled into the slits, thus increasing the total light power collected by the structure. In addition, the resonance enhancement factor of the optimized double-slit coupler is slightly larger than the resonance enhancement factor of the optimized single slit coupler. Overall, the use of an optimized double-slit coupler resulted in ~ 3.3 times enhancement of the coupling into the MDM plasmonic waveguide compared to the optimized single-slit coupler. We also found that, while the incoupling structures were all optimized at a single wavelength, the operation wavelength range for high coupling efficiency is broad.

As final remarks, for wavelength-scale slit-based structures the double-slit structure results in optimal coupling performance. We verified that, if three or more slits are used in a wavelength-scale coupler, the performance is always worse due to destructive interference between the waves coupled through the slits. Moreover, if a reflector is introduced in one of the two silver-silica-silver MDM output waveguides, then all the incoupled power will couple into the other silver-silica-silver MDM output waveguide. In addition, the proposed slit-based structures can also be used to couple light from a MDM plasmonic waveguide into free space. We found that, when the single slit structure is used to outcouple light, the radiation pattern of the structure is approximately isotropic [33]. On the other hand, we found that the two-section slit and double-slit structures introduce anisotropy in the radiation pattern, with stronger radiation in the normal direction [33]. Finally, we note that there are some analogies between the proposed coupling structures and the slot antennas used in the microwave frequency range [34].

Acknowledgments

This research was supported by the Louisiana Board of Regents (contracts LEQSF(2009-12)-RD-A-08 and LEQSF-EPS(2012)-PFUND-281), and the National Science Foundation (Award No. 1102301).